ASEN 3111
Computation of Lift and Drag
Computational Lab # 1
September 15, 2017

Nicholas Renninger, *

I. Introduction

Flow analysis can be a difficult task to surmount with only analytic techniques, so this lab is designed to develop some numeric solution techniques for basic classes of problems. More specifically, this lab focuses on the analysis of ideal (inviscid and incompressible) flow about certain airfoil geometries. These airfoil geometries, shown in Figure 2, were subjected to idealized flow conditions and the aerodynamic forces resultant on the airfoils were calculated numerically. For this lab, the only aerodynamic forces we concerned ourselves with were Lift per unit span ($L'\,[N/m]$) and Drag per unit span ($D'\,[N/m]$). The flow conditions for each problem were known (shown in Table 1), thus the determination of L' and D' was an exercise in analyzing the pressure distribution known about the airfoil, and integrating its effects to find the aerodynamic forces acting on the airfoil.

Table 1: Given Properties for Each Problem

Prob. #	$\boldsymbol{\alpha}$ $[^\circ]$	$\boldsymbol{V_\infty}$ $[m/s]$	$\boldsymbol{\rho_\infty}$ $[kg/m^3]$	$\boldsymbol{P_\infty}$ $[Pa]$	**c** $[m]$
1	0	25	0.9093	7.012×10^4	2
2	9	20	1.225	10.13×10^4	0.5

To find the equations for L' and D', we must first turn to Eqns. (1.7-1.8) in Anderson's text,[1] which define the normal (N') and axial (A') forces that act on an aerodynamic body. Because the flow is ideal, the shear forces (τ_u and τ_l) acting along the airfoil in these equations can be neglected. For the cylindrical airfoil shown in 2a, following the work shown in the figure leads to the reduction of the large equations for N' and A' in Anderson's text to the following:

$$L' = \oint_C -P\,sin(\theta)dS = R\int_0^{2\pi} -P\,sin(\theta)\,d\theta \;\text{ and }\; D' = \oint_C -P\,cos(\theta)dS = R\int_0^{2\pi} -P\,cos(\theta)\,d\theta \tag{1}$$

with $P = P(\theta)$ defined as:[4]

$$C_p(\theta) = \frac{P - P_\infty}{q_\infty} = 1 - 4sin^2(\theta) \quad \rightarrow \quad P = q_\infty C_p(\theta) + P_\infty \tag{2}$$

With these expressions for L', D' and C_p, we can begin the process of turning these integrals into discrete summations that can be more easily done on a computer. For problem 1, the Composite Simpson's Rule[3] was used to numerically approximate the values of the integrals in Eqn. (1)). Simpson's Rule uses a 2nd degree polynomial approximation, where each panel of the integration is defined by the area under a quadratic curve bounded by the start point, midpoint, and endpoint of each panel:[3]

$$F' \approx -R\frac{h}{3}\sum_{k=1}^{N/2}\left[f(\theta_{2k-1}) + 4f(\theta_{2k}) + f(\theta_{2k+1})\right], \quad h = 2\pi/N, \quad \theta_k = (k-1)h \tag{3}$$

*105492876

where for $F' = L'$, $f(\theta_k) = P(\theta_k)sin(\theta_k)$, for $F' = D'$, $f(\theta_k) = P(\theta_k)cos(\theta_k)$, and with N being the number of panels used in the integration. With Eqn. (3), the solution to finding both L' and D' is simply implemented on a computer, and accuracy is increased simply by increasing the N value (thus decreasing the effective step size of this iterative method). A more complete derivation of this Eqns. (1 - 3) can be found in Appendix A: Additional Figures and Tables.

Calculating L' and D' for the NACA 0012 airfoil is a little more involved in its derivation. Starting with Eqns. (1.7 - 1.8) from Anderson, then removing the shear stresses acting on the airfoil surface due to the assumption of ideal flow yield the following relationships for N' and A':

$$N' = -\int_{LE}^{TE} P_u(\theta)\, cos(\theta)\, ds_u + \int_{LE}^{TE} P_l(s)\, cos(\theta)\, ds_l \tag{4}$$

$$A' = \int_{LE}^{TE} P_u(s)\, sin(\theta)\, ds_u + \int_{LE}^{TE} P_l(s)\, sin(\theta)\, ds_l \tag{5}$$

To solve Eqns. (4 - 5) analytically, it would require an analytic expression for $P_u(s)$ and $P_l(s)$, which is beyond the scope of this lab document. Instead, the C_p data over the upper and lower airfoil surfaces is provided as a spline fit model developed using the vortex panel method.[4] that was developed Therefore, the Composite Trapezoidal Rule was used for numeric integration method of Eqns. (4 - 5). The Composite Trapezoidal Rule is much simpler than Simpson's Rule.[3] It is a linear approximation of the curve, where each panel of the integration is defined by the area under a linear curve bounded by the start point and endpoint of each panel (this area forms a trapezoid at each panel, hence the name). Based on the more extensive derivations found in Appendix A: Additional Figures and Tables, the distance between points used to define panel edges can be simplified to Δx for N' and Δy for A' and N' and A' become:

$$y_t(x) = \frac{t}{0.2} c \left[0.2969\sqrt{\frac{x}{c}} - 0.1260\left(\frac{x}{c}\right) - 0.3515\left(\frac{x}{c}\right)^2 + 0.2843\left(\frac{x}{c}\right)^3 - 0.1036\left(\frac{x}{c}\right)^4 \right] \tag{6}$$

$$N' = \sum_{k=1}^{N} - \left[\frac{P_u(x_{k+1}) - P_u(x_k)}{2} - \frac{P_l(x_{k+1}) - P_l(x_k)}{2} \right] \Delta x_k \tag{7}$$

$$A' = \sum_{k=1}^{N} \left[\frac{P_u(x_{k+1}) - P_u(x_k)}{2} + \frac{P_l(x_{k+1}) - P_l(x_k)}{2} \right] \Delta y_k \tag{8}$$

where y_t(x) defines the symmetric chord thickness of the NACA 0012 airfoil at every point along x. In order to transform N' and A' into the more conventional L' and D' required for this lab, Eqns. (1.1-1.2) from Anderson were used:[1]

$$L' = N'cos(\alpha) - A'sin(\alpha) \tag{9}$$

$$D' = N'sin(\alpha) + A'cos(\alpha) \tag{10}$$

Once the values for lift and drag have been computed for problem 2, the relative error of the result needs to be determined. This is first done by computing an "exact" value for L' (L_{exact}) using Eqns. (7 - 10) with a very large number of panels (I used 1×10^7, as shown in §II). Then, the relative error L_{err} can be computed using the following formula:

$$L_{err} = \frac{|L_{exact} - L_{calculated}|}{L_{exact}} \tag{11}$$

where $L_{calculated}$ is a function of the number of panels N used in its calculation in Eqns. (7 - 9). Eqn. (11) was used in conjunction with successive values for $L_{calculated}$ to determine the minimum number of panels needed for convergence below a given L_{err}.

To begin searching for the values of N that would result in the L_{err}, the search domain (N = [1, 10,000]) was broken into 100 non-uniform size steps. The larger number of steps at low N values, as seen in Figure

1, than at large N values was chosen to maximize efficiency; calculating successive values for L' and D' at large N is computationally expensive. Then a spline fit was applied to the rel. error, computed using Eqn. (11), at each of these 100 points so that interpolated values for the relative error could be found very quickly. These interpolated rel. error values were compared to the desired rel. error values, shown in Table 3, and the N values corresponding to matches between the fitted data and the required rel. errors were used as the starting points for an iterative search over N for the actual match with the fitted data. It is clear from Figure 1 that the fitted data search algorithm resulted in very fast and accurate determination of the actual N values, as shown by the small number of blue square points actually searched over the entire domain. The speedup this search algorithm provides is palpable, taking the run-time for problem 2 from several minutes on my computer to under 20 seconds (still using 1×10^7 panels and searching out to N = 10,000).

II. Results

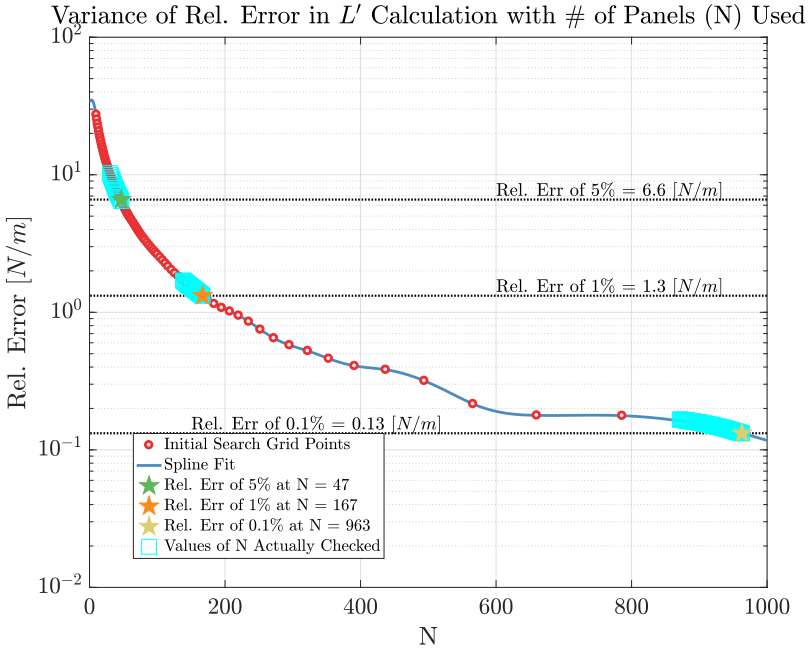

Figure 1: How relative error changes as the number of panels, N, increases. *The intersections of the rel. error curves and the blue fitted curve between the initial search grid points match very well with the actual value of N needed for the required rel. errors (shown as stars in the figure).*

Table 2: "Exact" L' and D' Calculations, computed using Eqn. (1 & 7 - 10)

Prob. #	**N Value Used** [# Panels]	$\boldsymbol{L'}$ $[N/m]$	$\boldsymbol{D'}$ $[N/m]$
1	1×10^7	$-3.33 \times 10^{-14} \rightarrow 0$	$1.08 \times 10^{-13} \rightarrow 0$
2	1×10^7	132.01	0.16283

Table 3: Number of Panels Needed for Given Rel. Err. & Accuracy of Initial Search Values

Rel. Error [%]	**Error Magnitude** $[N/m]$	**# Points Req.** [N]	**Est. # Points Req.** [N]	**Prediction Error** [%]
5	6.6	47	42	11.9
1	1.3	167	156	7.1
0.1	0.13	963	927	3.9

III. Conclusions

During the course of this computational lab, we developed equations for the lift and drag on airfoils using the fundamental aerodynamic force equations (Eqn. (1)). From these analytic, integral equations, numeric approximations methods for these integrals were used to allow for simpler calculation of the aerodynamic forces on the airfoils. However, as with any numerical analysis, convergence and accuracy are of primary concern, and can often be challenging to properly characterize. In this lab, we develop a simple methodology that allows for the approximate number of panels in the numeric integration process that are needed to achieve a certain degree of accuracy to a fully converged solution. By determining the minimum number of panels necessary for 0.1% relative error to a solution obtained with 1×10^7 panels, the efficiency of the integration calculation can be greatly increased. I chose to use 1×10^7 panels as my "exact" result because with so many panels, the convergence of the numeric solution is assured and unchanging as I could make it, which makes for the best possible reference value. I also used such a large number of panels as a way of stress testing the numeric integration and my search algorithm. As a fully converged solution with less than one percent error from "absolute" convergence can be obtained with less than 1000 panels, the number of panels used in normal calculations can be lowered for the computational domain of problem 2 without worry of loss of accuracy.

Besides the numeric analysis experience endowed by this problem, information about the aerodynamics of problems 1 and 2 can also be gleaned from this lab. For both problems 1 and 2, the flow was assumed to be ideal[4] (incompressible and inviscid). This proved to be a terrible assumption in the case of problem 1, but likely an acceptable assumption in the case of problem 2. As seen in Figure 3, the pressure distribution about the cylindrical airfoil was perfectly symmetric and indicated no loss of pressure due to separation at the rear ($x/c > 0.5$). Ideal flow about a solid body moving at constant velocity with respect to the flow is the very definition of D'Alembert's Paradox,[2] which perfectly describes the situation in problem 1. This lack of drag is obviously physically unreasonable, as we know from experience that blunt objects like a a cylinder experience massive amounts of pressure drag at large Reynolds numbers, as the flow easily separates from the body and forms a massive, lossy wake. However, as separation is impossible with viscosity, the inviscid assumption of the model used in problem 1 resulted in a very non-physical result. On the other hand, for slender, aerodynamic geometries like airfoils (the NACA 0012 in this case), the ideal flow assumption is a reasonable one. Airfoils experience generally small amounts of separation near the end of the chord length. This means that for the majority of the airfoil, flow is attached and generally follows a streamline about the airfoil. While the potential flow theory would still predict that the drag be 0 on the airfoil (all of the streamlines are continuous around the airfoil), numeric inaccuracy does not allow for this result in this lab. The lack of drag predicted by potential flow theory is still physically reasonable, as airfoils are designed to be slippery in the air. Lift is also accurately modeled, as potential flow theory still allows for lift on the airfoil. As α is positive, the flow is forced around the upper surface of the airfoil over longer streamlines, at a higher velocity than the flow around the bottom of the airfoil. This results in a net compression of the streamlines, which in turn creates a pressure gradient between the upper and lower surfaces, as seen in Figure 3. The integrated effect of this pressure force is lift. Therefore, the ideal flow model still allows for lift, but not drag, which are both physically meaningful assumptions to make.

The relative error results in this lab indicate that a minimum of 46 panels are needed to allow for the convergence of the numeric solver to within 5% of its converged value. This would correspond to having 46+ static pressure points on *both* the upper and lower surfaces of the airfoil, just to ensure that the ensuing numeric integration would be within 5% of its best result. This very large number of static pressure ports (over 100) is clearly unreasonable for such a small airfoil. Attempting to achieve 1% accuracy would require over 300 static pressure ports, and 0.1% accuracy would a completely ridiculous 1854+ ports to achieve the desired accuracy. These are non-physical numbers, and they mean that measuring the aerodynamic forces about a airfoil using static pressure rings will result in fairly low accuracy. Instead of measuring the aerodynamic forces using pressure ports along the airfoil, methods such as putting pressure ports along the wind tunnel test section surfaces or using a pitot rake (as described in Chapter 2 of Anderson[1]) should be utilized so that many more pressure ports may be realistically used. Also, another solution would be to experiment with more sophisticated integration models, especially ones involving higher-order polynomial approximation or spline approximations, that might result in faster convergence of the numeric solution (lower N value needed for the same accuracy). While the method used in this lab is simple and conceptually elegant, it has obvious practical limitations imposed by the numeric integration techniques used to approximate the lift and drag.

References

[1]Anderson, John D. Chapter 1, Part 1 Fundamentals of Aerodynamics, 5th ed., McGraw-Hill Education, 2011, pp. 20 - 23.
[2]Anderson, John D. Chapter 5 Introduction to Flight, 8th ed., McGraw-Hill Education, 2016
[3]Evans, John. ASEN 3111 Comp. Lab 1 Numeric Integration Slides. CU, 2017. PDF.
[4]Evans, John. ASEN 3111 Comp. Lab 1:"Calculation of Lift and Drag". Lab Document. CU, 2017. PDF.

Appendix A: Additional Figures and Tables

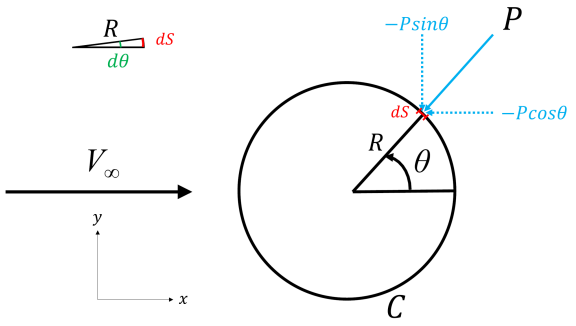

(a) Cylindrical Airfoil Geometry for Problem 1. *The figure illustrates the geometry of the problem ($\alpha = 0°$), as well as the basis for the derivation of L' and D' on the airfoil.*

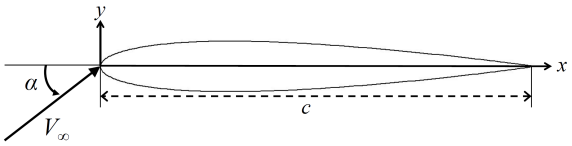

(b) NACA 0012 Airfoil Geometry used in Problem 2. *The NACA 0012 can clearly be seen to have symmetry (no camber) about its chord line. Note that $\alpha = 9° \neq 0°$, a different scenario than that of problem 1.*

Figure 2: Description and Definition of the Two Airfoil Geometries Analyzed

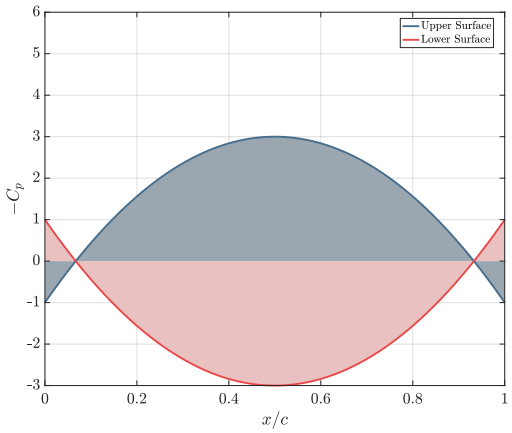

(a) Variation of C_p with chordwise position for the cylindrical airfoil. *As the pressure coefficient was obtained for ideal flow at $\alpha = 0°$,* the streamlines reconnect perfectly after going around the cylinder, so there is symmetric variation of pressure over the top and bottom surfaces as x/c increases. This symmetry, shown as the equal but opposite areas under the curves, means that there is no net lift on the airfoil. Also, as there is no loss of pressure due to separation on the back of the cylinder, there is symmetric pressure on both the front and back of the cylinder so there can be no pressure drag.

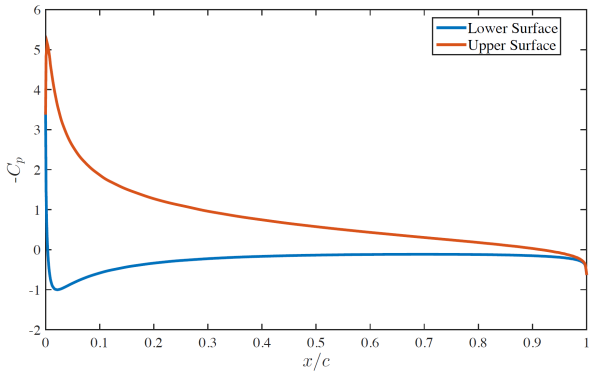

(b) Variation of C_p with chordwise position for the NACA 0012 airfoil. *Now, as $\alpha \neq 0°$, the pressure distribution about the upper and lower surfaces of the airfoil are no longer symmetric about the y-axis as x/c increases. As α is non-zero, we now have to consider A' and N' instead of L' and D'. As the area under the C_p curves is no longer symmetric as it was for the cylindrical airfoil, both A' and N' can no longer be 0. However, because the flow is inviscid, there still can be no drag on the airfoil, as there can be no flow separation along the airfoil to cause pressure losses between $x/c = [0, 1]$.*

Figure 3: Pressure Coefficients Over Upper and Lower Surfaces of Both Airfoils

Problem 1

$\oint_c f(\theta)\, ds$

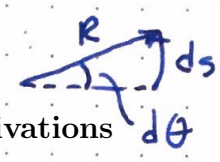

$ds = R\, d\theta$

$$\Rightarrow \oint_c f(\theta) R\, d\theta - R \oint_c f(\theta)\, d\theta$$

$$L' = R \int_0^{2\pi} -P(\theta) \sin\theta \, d\theta \qquad C_p = \frac{P(\theta) - P_\infty}{q_\infty}$$

$$C_p = 1 - 4\sin^2\theta$$

$$\rightarrow \quad 1 - 4\sin^2\theta = \frac{P - P_\infty}{q_\infty}$$

$$P = C_p q_\infty + P_\infty$$

$$P(\theta) = q_\infty - 4\sin^2\theta\, q_\infty + P_\infty \qquad \cancel{(C_p(\theta) q_\infty + P_\infty)}$$

$$L' = -R \int_0^{2\pi} (q_\infty - 4\sin^2\theta\, q_\infty + P_\infty) \sin\theta \, d\theta$$

Composite Simpson's Rule:

$$\int_a^b f(\theta)\, d\theta \approx \frac{h}{3} \sum_{k=1}^{N/2} \left[f(\theta_{2k-1}) + 4 f(\theta_{2k}) + f(\theta_{2k+1}) \right]$$

$$\theta_k = a + (k-1)h \quad , \quad h = \frac{b-a}{N}$$

$$\rightarrow L' = -R \int_0^{2\pi} \overbrace{(q_\infty - 4\sin^2\theta\, q_\infty + P_\infty)\sin\theta}^{f(\theta)} \, d\theta$$

$$L' \approx -R \, \tfrac{h}{3} \sum_{k=1}^{N/2} \left[f(\theta_{2k-1}) + 4 f(\theta_{2k}) + f(\theta_{2k+1}) \right]$$

$$\text{w/ } f(\theta) = (q_\infty - 4\sin^2\theta\, q_\infty + P_\infty)\sin\theta$$

$$L' = f(\theta)\,(C_p(\theta) q_\infty + P_\infty)\sin\theta$$

$$D' = f(\theta)\,(C_p(\theta) q_\infty + P_\infty)\cos\theta$$

Lab 1 - Comp - Problem 2

$$N' = N_u' + N_l'$$

$$N_u' = -\int_{LE}^{TE} (P_u \cos\theta + \cancel{\tau_u \sin\theta})^{\to 0} \, dS_u$$

$$= -\sum_{k=1}^{N} |\vec{x}_{k+1} - \vec{x}_k| \left(\left[\frac{P_u(\vec{x}_{k+1}) + P_u(\vec{x}_k)}{2} \right] C\theta_k \right)$$

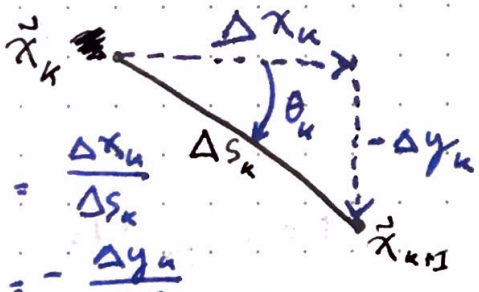

$$\cos\theta_k = \frac{\Delta x_k}{\Delta s_k}$$

$$\sin\theta_k = -\frac{\Delta y_k}{\Delta s_k}$$

$$\Delta s_k = |\vec{x}_{k+1} - \vec{x}_k|$$

$$\Delta x_k = x_{k+1} - x_k$$

$$\Delta y_k = y_{k+1} - y_k$$

$$N_u' \approx -\sum_{k=1}^{N} \Delta s_k \left(\frac{P_u(\vec{x}_{k+1}) + P_u(\vec{x}_k)}{2} \frac{\Delta x_k}{\Delta s_k} \right)$$

$$\approx -\sum_{k=1}^{N} \left(\frac{P_u(\vec{x}_{k+1}) + P_u(\vec{x}_k)}{2} \Delta x_k \right)$$

$$\therefore \quad N_l' \approx \sum_{k=1}^{N} \left(\frac{P_l(\vec{x}_{k+1}) + P_l(\vec{x}_k)}{2} \Delta x_k \right)$$

$$A' = A_u' + A_l' \Rightarrow A_u' = -\sum_{k=1}^{N} \left(\frac{P_u(\vec{x}_{k+1}) + P_u(\vec{x}_k)}{2} \Delta y_k \right)$$

$$A_l' = \sum_{k=1}^{N} \left(\frac{P_l(\vec{x}_{k+1}) + P_l(\vec{x}_k)}{2} \Delta y_k \right)$$

$$C_p = \frac{P - P_\infty}{q_\infty}$$

$$\Rightarrow \quad C_p q_\infty + P_\infty = P$$